JOURNAL OF AIRCRAFT
Vol. 38, No. 1, January–February 2001

Risk Analysis of Fuselage Splices Containing Multisite Damage and Corrosion

M. Liao* and Y. Xiong†
National Research Council of Canada, Ottawa, Ontario K1A 0R6, Canada

A risk analysis for fuselage splice joints containing multisite damage (MSD) and corrosion has been conducted using the software PRISM. The test data of crack growth history obtained using lap splice specimens were used in preparing the input data for PRISM and in validating the analysis. The MSD crack in the specimens was characterized by a single aggregate crack, and the median crack growth curve was derived and used in the analysis. The initial quality state of the splices was represented by an equivalent initial flaw size distribution, which was backtracked using the distribution of time to crack initiation. The critical crack length criterion was employed to predict the probability of failure (POF) at first linkup and final failure. The analysis results obtained are in good agreement with existing test data. It was found that the input data preparation played a key role in obtaining accurate predictions of POF.

Nomenclature

A	=	crack growth parameter
a	=	crack length
a_C	=	critical crack length
a_{cr}	=	aggregate crack length for the final failure
a_{EIFS}	=	equivalent initial flaw size
a_{lk}	=	aggregate lead crack length when the first linkup occurs
a_{TTCI}	=	crack length at time to crack initiation
B	=	crack growth parameter
b	=	crack growth parameter
C	=	crack growth parameter
$F_a(\cdots)$	=	cumulative distribution function of crack size
$f_a(a)$	=	probability density function of crack size
K	=	stress intensity factor
K_C	=	fracture toughness
Q	=	crack growth parameter
t_{TTCI}	=	time to crack initiation
X	=	lognormal random variable
$\beta(a)$	=	geometry factor
μ_{K_C}	=	mean of K_C
$\mu_{\ln t}$	=	mean of logarithm life
σ	=	far-fieled stress
σ_{K_C}	=	variance of K_C
$\sigma^2_{\ln t}$	=	variance of logarithm life
σ_M	=	standard deviation of material variability in crack growth
σ_{other}	=	standard deviation of other variable in crack growth
σ_U	=	standard deviation of usage variability in crack growth
σ_X	=	lognormal standard deviation of X
$\%P$	=	percentage of cracks that are found during inspection

I. Introduction

STRUCTURAL risk analysis predicts the probability of failure (POF) of structural components that are fatigue critical by taking into account various random factors associated with the initial quality state, material properties, loading, usage, inspection, and repair of the components. This technology has been increasingly used in the maintenance and management of aging aircraft fleets to improve flight safety and reduce costs. The output of risk analysis can be used to optimize the maintenance schedule of aging aircraft while maintaining the POF under an acceptable level.

To examine the performance of fatigue critical structures, probabilistic risk analysis has been applied to both military and commercial aircraft, and it is believed to be the approach of choice for the future.[1] Various probabilistic risk analysis methodologies have been developed for aging aircraft structures. Generally, there are two aspects in the probabilistic risk analysis to be noted.

First is deterministic damage tolerance and durability analysis, such as the analysis of the median crack growth data, the onset pattern of initial MSD, crack linkup criterion, and failure criterion. Considerable effort has been expended on this issue using fracture mechanics and finite element methods.[2,3]

Second are probabilistic methods to determine the POF, which is a joint probabilistic density function of multiple random factors. Usually, numerical integration methods (NIM),[2–4] Monte Carlo simulations,[5–7] the importance sampling method,[8] and the first-order reliability method[9,10] can be applied. In consideration of the small level of probabilities to be calculated, NIM are found to be ideal from the computational efficiency and robustness perspective.

In association with the methodologies discussed in the literature, several computer codes have been developed, such as PROF (U.S. Air Force),[3] NERF (Defence Science and Technology Organisation),[4] FEBREL (The Boeing Company),[8] PROMISS (Martec),[9] and NESSUS (Southwest Research Institute).[10] Bombardier Aerospace, Inc., has recently developed the code PRISM within the scope of the probabilistic system for the durability and damage tolerance analysis of aircraft structures contract from the Department of National Defence of Canada.[11,12] The code can be used to calculate the POF within a single flight or an inspection interval of flights accounting for the inherent variability in the initial quality state, material, loading, inspection and repair action, and usage of the components. An evaluation of PRISM has been conducted by the authors using PROF as a benchmark code.[13] It has been found that PRISM and PROF have different merits, but both provide comparable results.

This paper presents some results of a risk analysis conducted using PRISM for lap joint specimens tested under a separate program. The specimens were designed to simulate longitudinal fuselage splices in a transport aircraft that are typical fatigue critical structures in which multisite damage (MSD) develops with flight hours. Unlike a single crack, MSD in a structure can result in a significant reduction in fatigue life. The test program was carried out at the Institute for Aerospace Research of the National Research Council Canada (IAR/NRC) to investigate the fatigue characteristics of

Received 10 February 2000; revision received 31 July 2000; accepted for publication 3 August 2000.

*National Sciences and Engineering Research Council of Canada Research Fellow, Structural, Materials and Propulsion Laboratory, Institute for Aerospace Research. Member AIAA.

†Research Officer, Structural, Materials and Propulsion Laboratory, Institute for Aerospace Research. Member AIAA.

fuselage splices containing MSD and corrosion.[14,15] Extensive test data for noncorroded and corroded specimens were obtained. Corrosion pillowing in splice joints was also studied, and its role in the development of fatigue damage and other forms of cracking was recognized.[16,17] Based on the test data, a cost-effective methodology for probabilistic analysis of fuselage splices has been proposed by Xiong and Shi[6] and Xiong et al.[7] using Monte Carlo simulations. The test data supplied by IAR/NRC were also used to verify the risk assessment work by Berens et al.[3] (also see Ref. 2) based on finite element analysis and deterministic crack growth analysis.

In this work, a median crack growth curve along with the equivalent initial flaw size distribution (EIFSD) was used, and a critical crack length criterion was employed to predict the POF. These input data for PRISM were derived from the test data, and in doing so, sophisticated finite element analysis was avoided for calculation of crack parameters. In the following sections, the geometry configuration and the failure characteristics of the specimens are described, the methodologies used in PRISM are briefly reviewed, and the input data preparation that plays a key role in accurate prediction of POF is discussed in detail. Analysis results are presented, and the influences of corrosion on the risk level of MSD specimens are examined.

II. Specimen Configuration and Failure Characteristics

Figure 1 shows the material and the geometry of the splice specimen developed by IAR/NRC. The specimen was constructed of two 0.040-in. (1.0-mm) sheets of 2024-T3 clad aluminum with three rows of 5/32-in. (4-mm) 2117-T4 rivets (MS20426AD5-5). The section cut in Fig. 1 shows the countersink geometry of the rivet holes, which form a knife edge in the outer panel of the splice. The design of the specimen was based on a proven concept for a uniaxial splice test specimen that simulates aircraft fatigue conditions.[17]

Fatigue tests were conducted using constant amplitude fatigue loading of 12.89 ksi (88.9 MPa) with stress ratio $R = 0.2$ and a frequency of 8 Hz. Test results for the fatigue life of nine noncorroded and five corroded (2–4% thickness loss) specimens are presented in Table 1. From Table 1, a significant difference was noted in the behavior of the splice specimens with and without corrosion. The mean life to final failure was reduced by 26% due to corrosion. The scatter of fatigue life of the corroded specimens was much smaller than that of the noncorroded specimens. The scatter in the test results were primarily sourced from materials, manufacturing, riveting, and assembly. Furthermore, Table 1 indicated that the load cycle to first linkup of two lead cracks in the noncorroded specimens occupied 98% of their total fatigue life, and similar behavior was observed in the corroded specimens.

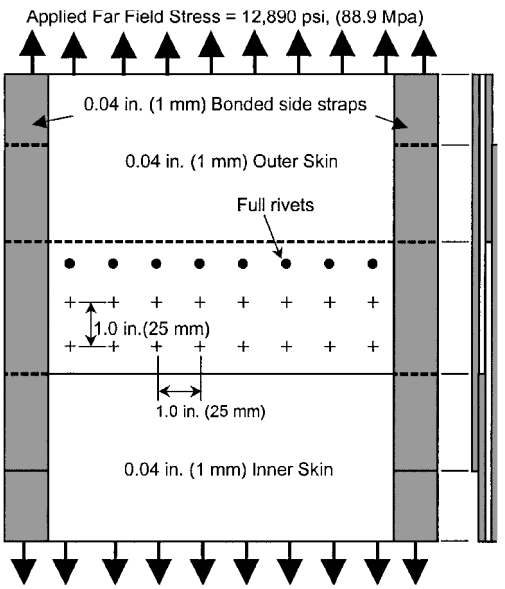

Fig. 1 IAR/NRC lap splice specimen configuration.[2,14]

Table 1 Fatigue life of the splice specimens

Specimen	Fatigue life (cycles) 1st Linkup	Final failure
	G1 group	
Cgc-f0	405,902	412,575
Cgc-f1	362,500	368,335
Cgc-f3	228,500	231,050
Cgc-f4	255,600	260,400
Cgc-f5	173,452	176,957
Cgc-f6	436,940	441,333
Cgc-f7	250,800	259,180
Cgc-f8	292,700	298,550
Cgc-f9	199,850	203,075
Mean	**289,583**	**294,606**
Standard deviation	**92,533**	**93,261**
Coefficient of variation, %	**32.0**	**31.7**
	G3 group	
Cgc-cf1	211,000	221,600
Cgc-cf3	194,300	196,850
Cgc-cf4	221,800	225,600
Cgc-cf5	173,500	185,100
Cgc-cf6	254,700	258,900
Mean	**211,060**	**217,610**
Standard deviation	**30,461**	**28,603**
Coefficient of variation, %	**14.4**	**13.1**

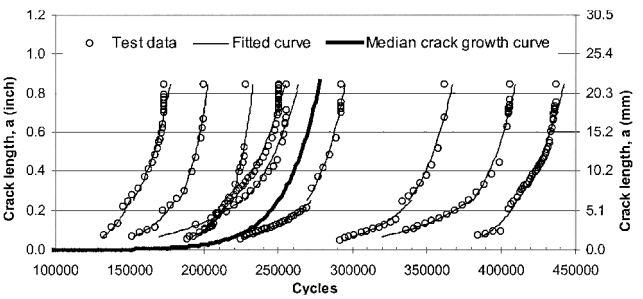

Fig. 2 CG data for noncorroded specimens (aggregate lead crack).[6,7]

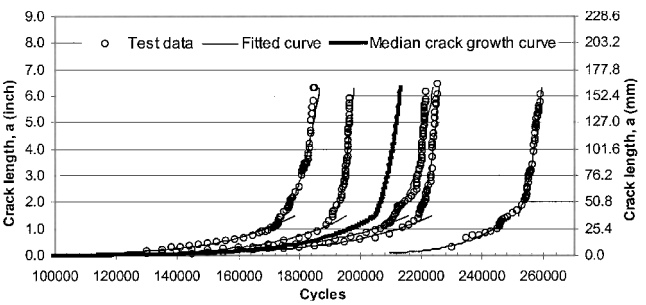

Fig. 3 CG data for corroded (2–4% thickness loss) specimens (aggregate crack).[6,7]

Although different MSD scenarios were observed in the tests, basically MSD tends to develop in clusters within the boundaries of a frame bay. Similarly, the linkup of MSD and the formation of a lead crack also tend to occur initially within a frame bay. For this reason, it can be helpful to view the MSD test data as an aggregate crack growth curve. In this paper, two kinds of aggregate cracks were used to characterize MSD cracks. For the noncorroded specimens, the lengths of the two lead cracks in the failed ligament were added together and were treated as a single crack called the aggregated lead crack. For the corroded specimens, all individual crack lengths along the rivet row were added together and called the aggregate crack.

The test data of crack growth history of the two specimen groups are shown in Figs. 2 and 3, respectively. For noncorroded specimens (Fig. 2), crack growth was relatively faster after the aggregate lead crack length reached about 0.2–0.25 in. (5.1 ~ 6.35 mm). In the five

corroded specimens (Fig. 3), the first linkup occurred at an aggregate crack length of about 1.5 in. (38.1 mm), and the subsequent crack growth was much faster and became unstable.

In this work, two different failure conditions are considered for noncorroded and corroded specimens. First, the noncorroded specimen is considered to have failed when the first linkup occurs at which time the length of the aggregate lead crack reaches a specific value a_{lk}, which is the length of the ligament $a_{lk} = 0.844$ in. (21.4 mm). Second, the corroded specimen is considered to have failed when the aggregate crack length reaches a critical value a_{cr}. The critical crack length for final failure is taken from the mean value of the crack lengths obtained from corroded test data corresponding to failure life, that is, $a_{cr} = 6.16$ in. (156.5 mm) (Refs. 6 and 7).

III. Analysis Methodologies in PRISM

A brief review of the methodologies used in PRISM is given in this section. The risk analysis framework of PRISM is shown in Fig. 4.

A. Initial Crack State

PRISM provides two types of initial crack states: One is a single crack size, which must be used along with a stochastic crack growth model. The other one is an initial crack size distribution (ICSD). The present version of PRISM has 10 optional statistical distributions for the ICSD, as listed in Table 2, which are all commonly used distributions in engineering. These 10 distributions must be input in a closed-form format.

B. Median Crack Growth Curve

PRISM can use either a deterministic or a stochastic crack growth (CG) model in the risk analysis. To consider the randomness in CG the Yang and Manning stochastic CG model[18] is employed for the median CG curve. The deterministic CG model is expressed as

$$\frac{da(t)}{dt} = Q[a(t)]^b \tag{1}$$

Table 2 PRISM: 10 optional statistical distributions

Number	Distribution
1	Beta
2	Exponential
3	Gumble (extreme value)
4	Log-logistic
5	Lognormal (2 parameter)
6	Normal
7	Undefined[a]
8	Uniform
9	Weibull (3 parameter)
10	Weibull compatible

[a]Not applicable in the present version.

where $a(t)$ is the crack size at time t. The stochastic CG model is expressed as

$$\frac{da(t)}{dt} = XQ[a(t)]^b \tag{2}$$

where X has a median of 1.0 and a lognormal standard deviation σ_X, which is a combination of the scatters associated with material, σ_M, usage, σ_U, and others, σ_{other},

$$\sigma_X = \sqrt{\sigma_M + \sigma_U + \sigma_{other}} \tag{3}$$

C. Geometry Factor

In PRISM, the stress intensity factor K is defined as a function of the stress and the crack size expressed as

$$K = \sigma \cdot \sqrt{\pi a} \cdot \beta(a) \tag{4}$$

where $\beta(a)$ is the geometry factor that is the function of crack size a.

D. Probability of Detection [POD(a)]

PRISM uses the probability of detection (POD) as a function of the crack size, POD(a), to represent the capability of the inspection techniques. In PRISM, POD(a) can be modeled by 10 optional distributions (as shown in Table 2).

E. Maximum Stress Distribution

PRISM uses the maximum stress distribution to reflect the scatter of spectrum loading and provides 10 optional distributions (Table 2) for the maximum stress distribution.

F. Failure Criterion

PRISM applies two failure criteria based on the critical crack length a_C and the fracture toughness K_C to calculate the POF. The two criteria are written as follows.

Critical crack length criterion:

$$\text{POF} = P(a \geq a_C) \tag{5}$$

Fracture toughness criterion:

$$\text{POF} = P(K \geq K_C) \tag{6}$$

PRISM allows users to choose 10 optional distributions (Table 2) for the fracture toughness K_C.

G. POF Calculation

PRISM can calculate two types of POF. One is the POF at a specified crack size POF(a), which is expressed as

$$\text{POF}(a) = \int_0^\infty f_{K_C}(K_C)\hat{H}[\sigma_C(a, K_C)]\,dK_C \tag{7}$$

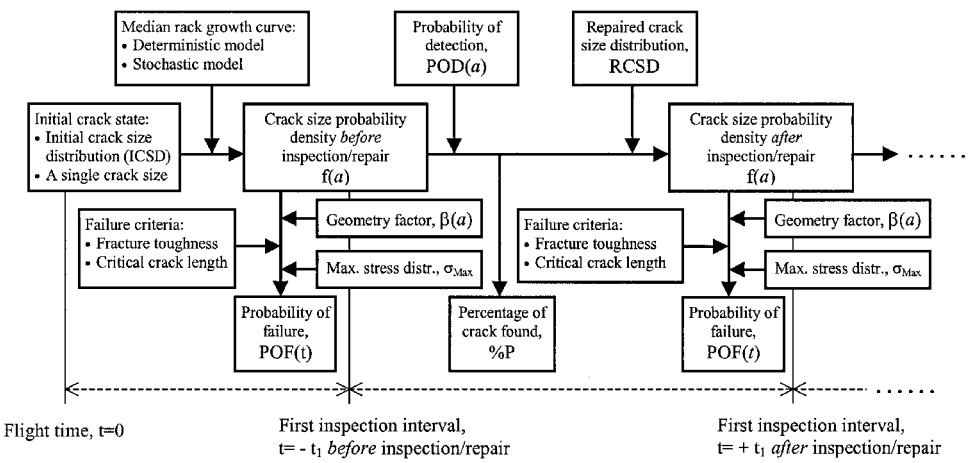

Fig. 4 Schematic flowchart of PRISM.

where $f_{K_C}(K_C)$ is the probability density function of K_C, $\hat{H}[\sigma] = 1 - H(\sigma)$ is the exceedance probability distribution function for the maximum stress in a single flight, $H(\sigma)$ is the distribution of the maximum stress per flight, and $\sigma_C(a, K_C) = K_C/[\sqrt{(\pi a)}\beta(a)]$ is the critical stress at a given crack size and K_C.

The other POF calculated by PRISM is the POF for a defined inspection interval or flight hours, POF(t). When the user selects the a_C criterion, POF(t) is expressed as

$$\text{POF}(t) = \int_{a_C}^{\infty} f_a(a)\,\mathrm{d}a = 1 - F_a(a_C) \tag{8}$$

where $f_a(a)$ is the PDF of crack size and $F_a(\cdots)$ is the cumulative distribution function (CDF) of a. When the user selects the K_C criterion, POF(t) is expressed as

$$\text{POF}(t) = \int_0^{a_C} f_a(a) \int_0^{\infty} f(K_C)\hat{H}[\sigma_C(a, K_C)]\,\mathrm{d}K_C\,\mathrm{d}a$$

$$+ [1 - F_a(a_C)] = \int_0^{a_C} f_a(a)\text{POF}(a)\,\mathrm{d}a + [1 - F_a(a_C)] \tag{9}$$

which accounts for the probability that the crack length is greater than a_C and the probability that the crack length is smaller than a_C, but a stress greater than σ_C is encountered during the usage interval. As a matter of fact, Eq. (9) employs a combination of a_C and K_C failure criteria.

H. Inspection and Repair Calculation

The capability of an inspection to find a crack at a detail at a certain time t is determined by the POD curve as well as the crack size distribution. The inspection involves determining an important output, that is, the percentage of cracks that are found during an inspection, which is written as

$$\%P = \int_0^{\infty} \text{POD}(a)\, f_{a,\text{before}}(a)\,\mathrm{d}a \tag{10}$$

where $f_{a,\text{before}}(a)$ is the PDF of crack sizes just before a maintenance.

Once a crack is detected, the detail is usually repaired to remove the crack. The repair quality is expressed in terms of the repaired crack size distribution (RCSD), $f_R(a)$. Because the data of the RCSD is very limited, an assumed RCSD, similar to the ICSD, is usually used in PRISM. The crack distribution after the inspection and repair, $f_{a,\text{after}}(a)$, is then given by

$$f_{a,\text{after}}(a) = \%P f_{\text{RCSD}}(a) + [1 - \text{POD}(a)]F_{a,\text{before}}(a) \tag{11}$$

where $f_{\text{RCSD}}(a)$ is the PDF of the RCSD. In Eq. (11), the first term represents the repaired detail with a specific distribution when they are repaired, whereas the second term accounts for the nondetected and nonrepaired details with the same distribution as before the inspection.

In summary, PRISM provides various methods for risk analysis with optional features associated with the initial crack state, CG model, and failure criterion. These methods are as follows: 1) single crack size plus stochastic CG model plus K_C criterion, 2) single crack size plus stochastic CG model plus a_C criterion, 3) ICSD plus deterministic CG model plus K_C criterion, 4) ICSD plus deterministic CG model plus a_C criterion, 5) ICSD plus stochastic CG model plus K_C criterion, and 6) ICSD plus stochastic CG model plus a_C criterion.

IV. Input Data Preparation

A. Median CG Curve

In this work, the median CG curve was taken from the test data by a curve fitting. For better curve fitting, the CG curves were divided into two regions, and the division points were set at a crack length of 0.25 in. (6.35 mm) for noncorroded specimens and 1.5 in. (38.1 mm) for corroded specimens. Different CG equations were applied in regions 1 and 2 as follows.

Region 1:

$$a = Ae^{Bt} \tag{12}$$

Region 2:

$$\frac{\mathrm{d}a}{\mathrm{d}t} = Q[a(t)]^b \tag{13}$$

There are two reasons to apply an exponential function to describe CG in region 1. One is that the small CG in region 1 can be described very well by an exponential function, and the other reason is the EIFSD can be easily backtracked using an exponential function. In addition, Eq. (12) can be converted to Eq. (13) when $Q = B$ and $b = 1$.

To reduce the statistical variability due to a different number of data points, that is, different weight, on each CG curve, an equal number of data points for each curve was generated to calculate the CG parameters. The fitted curves were calculated using Microsoft Excel and are presented in Figs. 2 and 3 along with the test data. The parameters of the median CG curves for noncorroded and corroded specimens were also calculated using Microsoft Excel and are listed in Table 3. The median CG curves appear to represent well the median behavior of the test data (Figs. 2 and 3).

B. Initial Crack Size Distribution

The EIFSD used in this work was calculated from the distribution of time to crack initiation (TTCI). The assumed relationship between an EIFS, a_{EIFS}, and a TTCI, t_{TTCI}, is represented by a deterministic crack growth equation,

$$a_{\text{EIFS}} = g(t_{\text{TTCI}}, a_{\text{TTCI}}, C) \tag{14}$$

where a_{TTCI} is the crack size at t_{TTCI} and C represents a set of CG parameters, which are constants. For fatigue CG, a_{EIFS} is always a monotonic decrease function of t_{TTCI} when a_{TTCI} is fixed. From probability theory, the CDF of a_{EIFS} is given by

$$F_a(a_{\text{EIFS}}) = 1 - F_t[h(a_{\text{EIFS}}, a_{\text{TTCI}}, C)] \tag{15}$$

where $h(a_{\text{EIFS}}, a_{\text{TTCI}}, C)$ is the inverse function of $g(a_{\text{EIFS}}, a_{\text{TTCI}}, C)$ and $F_a(\cdots)$ and $F_t(\cdots)$ are the CDF of a_{EIFS} and t_{TTCI}, respectively.

In this work the crack length at the starting time was defined as $a_{\text{TTCI}} = 0.08$ in. (2.032 mm) for both noncorroded and corroded specimens. This crack length is visible in a test, and therefore, crack initiation actually means the formation of a visible crack. Then the TTCI data were obtained from each specimen using the fitted crack growth curve [region 1, Eq. (12)] and listed in Table 4. Moreover the

Table 3 CG parameters for PRISM

Region	$a_{\min}$	$a_{\max}$	Q	b	σ_M	σ_U	σ_{other}	σ_X
Noncorroded specimens								
1	1e−4	0.25	4.4828e−05	1	0.0	0.0	0.0	0.0
2	0.25	0.844	4.6166e−05	0.9783	0.266	0.0	0.0	0.266
Corroded specimens (2–4% thickness loss)								
1	1e−4	1.5	4.7865e−05	1	0.0	0.0	0.0	0.0
2	1.5	6.26	1.7568e−4	1.0001	0.295	0.0	0.0	0.295

Table 4 TTCI data at $a_{\text{TTCI}} = 0.08$ in. (2.03 mm)

Number	Noncorroded specimen (cycles)	Corroded specimen (cycles)
1	134,099.8	113,958.1
2	156,280.5	131,022.8
3	176,134.1	134,306.3
4	195,231.0	145,575.2
5	221,294.6	209,992.0
6	233,417.0	——
7	305,476.3	——
8	327,814.8	——
9	390,352.4	——
Mean	**237,788.9**	**146,970.9**
Standard deviation	**86,067.2**	**37,007.4**
c.v., %	**36.2**	**25.2**

TTCI data were checked by the Anderson–Darling goodness-of-fit test (see Ref. 19). The following lognormal distributions were found to fit the TTCI data best as compared to the normal and Weibull distributions:

$$F_{\mathrm{TTCI}}(t) = \Phi\left[\left(\ell n t - \mu_{\ell n t}\right)\Big/\sigma_{\ell n t}\right] \tag{16}$$

where $\mu_{\ell n t}$ and $\sigma^2_{\ell n t}$ are the mean and variance of $\ell n\, t$. For noncorroded specimens, $\mu_{\ell n t} = 12.322$ and $\sigma_{\ell n t} = 0.3572$, whereas for corroded specimens, $\mu_{\ell n t} = 11.876$ and $\sigma_{\ell n t} = 0.2296$. Figure 5 presents the distributions of TTCI for the noncorroded and corroded specimens. When the median crack growth curve defined by Eq. (12) is substituted into Eq. (15), the EIFSD is derived as

$$F_a(a_{\mathrm{EIFS}}) = 1 - \Phi\left\{\frac{\ell n[(1/B)\ell n(a_{\mathrm{TTCI}}/a_{\mathrm{EIFS}})] - \mu_{\ell n t}}{\sigma_{\ell n t}}\right\} \tag{17}$$

From Eq. (17), tabular data (a_i and P_i) for the EIFSD were calculated. Figure 6 presents data (a_i and P_i) and provides a comparison of the EIFSD for noncorroded and corroded specimens. A two-parameter Weibull distribution was found to fit these tabular data best as compared to the lognormal, Weibull compatible and normal distributions. Table 5 presents the Weibull parameters of EIFSD for PRISM.

Table 5 Weibull parameters of EIFSD for PRISM

Specimen	Shape parameter, α	Scale parameter, β
Noncorroded	0.328511	1.0364e−05
Corroded	0.726981	1.4857e−4

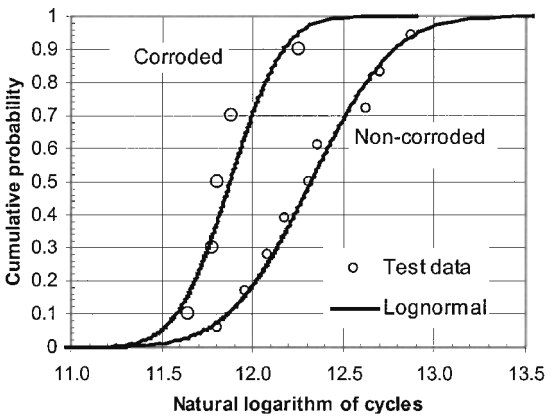

Fig. 5 TTCI distributions for noncorroded and corroded specimens.

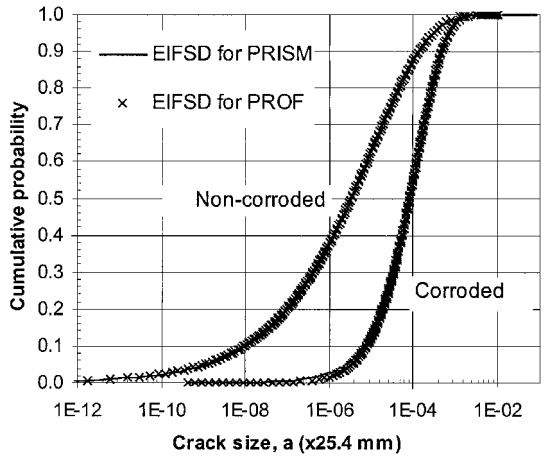

Fig. 6 EIFSD for noncorroded and corroded specimens.

Table 6 Gumbel parameters for maximum stress distribution, ksi or × 6.895 Mpa

Corrosion, %	Mean	Standard deviation	Gumbel A deviation	Gumbel B deviation
0	12.89	0.6445	0.5025	13.18
2–4	13.15	0.6575	0.5126	13.45

C. Critical Crack Length

The noncorroded specimens were considered to have failed when the first linkup occurred or when the aggregate lead crack reached a specific length of a_{lk}. The corroded specimens were considered to have failed when the aggregate crack length reached a critical value of a_{cr}. In this work, the critical crack length for the first linkup and the final failure were taken from test data as $a_{\mathrm{lk}} = 0.844$ in. (21.4 mm) and $a_{\mathrm{cr}} = 6.16$ in. (156.5 mm), respectively.[6,7]

D. Fracture Toughness Distribution

For the 0.04-in.(1-mm) sheet of 2024-T3 clad aluminum, the fracture toughness distribution was assumed to follow a normal distribution with a mean and standard deviation of $\mu_{K_C} = 138$ ksi $\sqrt{(\mathrm{in.})}$ [151.6 MPa$\sqrt{(\mathrm{m})}$] and $\sigma_{K_C} = 5$ ksi$\sqrt{(\mathrm{in.})}$[5.5 MPa$\sqrt{(\mathrm{m})}$], respectively.[2,3] Because this example used the critical crack length criterion, the K_C criterion had no influence on the POF calculation. The input of K_C distribution was needed just to run the software.

E. Geometry Factor

Because the K_C criterion had no influence on the risk analysis in this work, the geometry factors were arbitrarily set to be small so that the K_C criterion would not affect the calculated results. However, the last crack length a_{last}, a parameter in the input data of geometry factor, was needed by PRISM. In this paper, a_{last} (or a_{limit} in PRISM) was also set to 0.844 in. (21.4 mm) and 6.16 in. (156.5 mm) for noncorroded and corroded specimens, respectively.

F. Maximum Stress Distribution

The Gumble extreme value distributions with a mean at the constant amplitude level in test and a small standard deviation were used for the maximum stress distribution. Table 6 presents the Gumble parameters for noncorroded and corroded specimens, which were calculated in Ref. 2 by taking into account the material loss due to corrosion. Similarly, the maximum stress distribution had an insignificant effect on the risk analysis because the critical crack length criterion was applied in this example.

G. POD(a) and RCSD

Because the present risk analysis does not involve any inspection and repair activities, arbitrary but reasonable data were used to define the POD(a) and the RCSD.

V. Results

Using the prepared input data, PRISM was run to calculate the POF of the MSD specimens. For the purpose of comparison, the software PROF was also run to predict the POF using the same set of input data. Figure 7 presents the calculated POF(t) by PRISM and PROF vs load cycles for noncorroded and corroded specimens. In Fig. 7, the POF values of the test sample are determined by the nonparametric estimate of the ordered test sample,[20] that is, $(i - 0.5)/n$. It is seen that the results from PRISM and PROF are close to each other and are in reasonably good agreement with the test data for both noncorroded and corroded specimens. It is also noted that the POF(t) results of corroded specimens at the 2–4% level are much higher than those of non-corroded specimens at the same load cycle, that is, corrosion in splices, even at a low level, can result in a significant reduction in fatigue life.

To examine the influence of input data preparation on the accuracy of POF predictions, different input data were used in PRISM and PROF and the calculations repeated. PRISM allows the user to divide

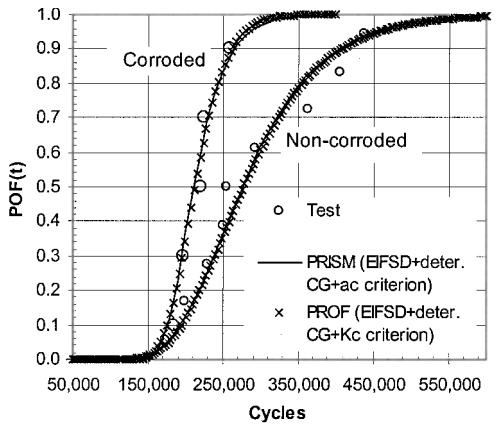

Fig. 7 POF calculated by PRISM and PROF.

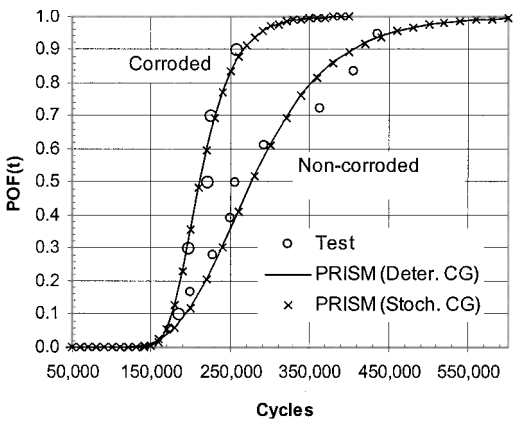

Fig. 8 POF calculated by PRISM using different CG curves.

the CG period into multiple regions and to use either deterministic or stochastic CG models for each region. As a demonstration, Fig. 8 shows the POF(t) calculated by PRISM using deterministic and stochastic CG models for noncorroded and corroded specimens. In the stochastic CG, only the scatter in region 2 was considered, with the scatter in region 1 being accounted for in the determination of EIFSD. It is seen that using a stochastic CG model did not produce different POF(t) results in this work. That is because the scatter in region 2 of CG had almost no contribution to the entire fatigue process. In other words, the EIFSD dominated the POF(t) calculations.

Because the EIFSD was calculated from the TTCI data, the TTCI distribution must have had a great effect on the POF(t) results. To demonstrate this, a mixed TTCI distribution and EIFSD were used in PROF to calculate the POF of the noncorroded specimens because the present version of PRISM does not support a mixed distribution for the optional distributions as listed in Table 2. For the noncorroded specimens, a mixture of Weibull distributions was derived to fit the TTCI data as

$$F_{\text{mixed TTCI}}(t) = \tfrac{2}{3}\left\{1 - \exp\left[-(t/\beta_1)^{\alpha_1}\right]\right\} + \tfrac{1}{3}\left\{1 - \exp\left[-(t/\beta_2)^{\alpha_2}\right]\right\}$$

$$= 1 - \tfrac{2}{3}\exp\left[-(t/\beta_1)^{\alpha_1}\right] - \tfrac{1}{3}\exp\left[-(t/\beta_2)^{\alpha_2}\right] \quad (18)$$

where $\alpha_1 = 5.6156$, $\beta_1 = 200{,}949$ and $\alpha_2 = 8.583$, $\beta_2 = 359{,}594$. Figure 9 shows this mixed distribution of TTCI for noncorroded specimens. It is seen that the mixed Weibull distribution provides a better fit to the TTCI data as compared to the lognormal distribution. With the use of the preceding approach, a mixed EIFSD was calculated, from the mixed TTCI distribution. Then the POF(t) was calculated, and the results are shown in Fig. 10. It is seen that the mixed EIFSD significantly improved the POF(t) prediction in PROF as compared with the results from other approaches.

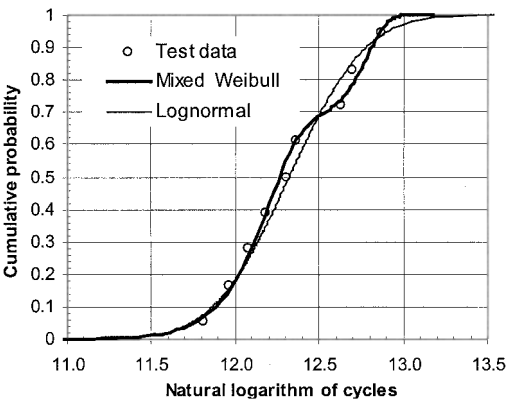

Fig. 9 TTCI distribution for noncorroded specimens.

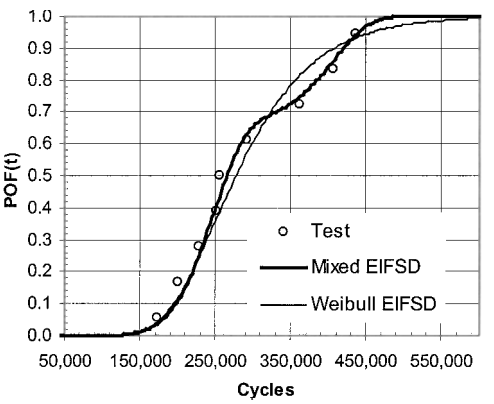

Fig. 10 POF of noncorroded specimens using various EIFSD.

VI. Conclusions

A risk analysis has been conducted for lap splice specimens containing MSD and corrosion using the software PRISM developed by Bombardier Aerospace, Inc. The U.S. Air Force code PROF was used as benchmark software. For the specimens considered, PRISM provided almost identical POF results to those from the benchmark software PROF, and the results were in good agreement with the test data. PRISM is found to be an easy to use and capable tool for probabilistic durability and damage tolerance analysis and risk assessment for aging aircraft.

Characterization of the MSD in lap splices using a single aggregate crack appears to be a useful simplification in conducting risk analysis. The curve fitting to the test data developed by IAR/NRC provided accurate input data for PRISM and PROF. In this way, the necessity for sophisticated finite element crack growth analysis was avoided. Therefore, a proven risk assessment code with limited test data might be a practical and cost-effective way to conduct risk analyses of fuselage splices containing MSD, especially for a corroded structure because corrosion/fatigue interaction mechanisms are not clear at present time. Corrosion in lap splices can have a significant influence on the probability of failure of the structure.

The accuracy of the POF predictions of the MSD specimens was also found to be largely influenced by the EIFSD used. A significant improvement in the POF prediction can be achieved using the EIFSD input derived from accurate TTCI distributions.

Acknowledgments

This work has been carried out under Institute for Aerospace Research Program 303 Aerospace Structures, Project 46_QJ0_24, Reliability Analysis and Risk Assessment of Aerospace Structures. The financial assistance received from Department of National Defence of Canada is gratefully acknowledged. Thanks are extended to Simon Kaczor of Bombardier Aerospace, Inc., for providing the latest version of PRISM and useful discussions on PRISM, to G.

Eastaugh of the National Research Council of Canada and P. V. Straznicky of Carleton University for providing the raw test data, and to A. P. Berens of University of Dayton Research Institute and Peter Hovey of the U.S. Air Force Research Laboratory for their helpful discussions on PROF. Finally, special thanks are extended to the Associated Editor and Reviewers of this paper.

References

[1]Lincoln, J. W., "Overview of Widespread Fatigue Damage: Risk Assessment Methodology," CP-568, AGARD, 1995, pp. 1-1–1-11.

[2]Cope, D., "Corrosion Damage Assessment Framework," The Boeing Co., Rept. D500-13008-1, Seattle, WA, Aug. 1998.

[3]Berens, A. P., West, J. D., and Trego, A., "Risk Assessment of Fatigue Cracks in Corroded Lap Joints," *Fatigue in the Presence of Corrosion, Proceedings of the Research and Technology Organisation of North Atlantic Treaty Organization Meeting Proceedings 18*, Neuilly-Sur-Seine Cedex, France, 1998, pp. 21-1–21-10.

[4]Graham, D., Mallinson, G. D., and Tong, C., "NERF—A Tool for Aircraft Structural Risk Analysis," *Proceedings of the International Conference on Applications of Statistics and Probablity*, Dec. 1999, pp. 1175–1190.

[5]Shinozuka, M., Deodatis, G., Sampath, S., and Asada, H., "Statistical Property of Widespread Fatigue Damage," CP-568, AGARD, 1995, pp. 7-1–7-12.

[6]Xiong, Y., and Shi, G., "A Stochastic Damage Growth Model for Failure Prediction of Fuselage Splice Joints with Multiple-Site Damage," Inst. for Aerospace Research, Rept. LTR-ST-2152, National Research Council of Canada, Ottawa, April 1999.

[7]Xiong, Y., Eastaugh, G., and Shi, G., "Probabilistic Failure Analysis of Fuselage Splice Joints with Multiple Site Fatigue Damage and Corrosion," *Proceedings of the International Conference of Aeronautic Fatigue*, Engineering Materials Advisory Services, Ltd., Cradley Heath, U.K., 1999.

[8]Torng, T. Y., and Edwards, R. M., "Comparing B-1B Wing Carry Through Inspection Requirements as Defined by Deterministic and Probabilistic Approaches," *Proceedings of 1998 USAF Aircraft Structural Integrity Program Conference*, 1998.

[9]Orisamolu, I. R., Lou, X., and Lichodziejewski, M., "Development of Probabilistic Optimal Strategies for Inspection/Monitoring/Maintenance/Repair and Life Extension," Martec, Ltd., Halifax, Canada, TR SRV-6-00251, 1999.

[10]"Probabilistic Analysis and Design," *9th Annual Short Course Notes*, Southwest Research Inst., San Antonio, TX, 1998.

[11]Forges, S. A., "PRISM User's Guide," Rept. RAZ-DSD-101, Bombardier Aerospace, Montreal, Canada, Defence Services, 1997.

[12]Kaczor, S., and Sarrazin, G., "Updated PRISM User's Guide," Bombardier Aerospace, Inc., Montreal, Canada, Defence Services, 2000 (to be published).

[13]Liao, M., and Xiong, Y., "PRISM—A Computer Code for Risk Assessment of Aging Aircraft Structures," Inst. for Aerospace Research, Rept. LTR-ST-2248, National Research Council of Canada, Ottawa, Nov. 1999.

[14]Eastaugh, G. F., Simpson, D. L., Straznicky, P. V., and Wakeman, R. B., "A Special Uniaxial Coupon Test Specimen for the Simulation of Multiple Site Fatigue Crack Growth and Linkup in Fuselage Splices," CP-568, AGARD, 1995, pp. 2-1–2-19.

[15]Scott, J. P., "Corrosion and Multiple Site Damage in Riveted Fuselage Lap Joints," M.S. Thesis, Dept. of Mechanical and Aerospace Engineering, Carleton Univ., Ottawa, Canada, 1997.

[16]Eastaugh, G. F., Merati, A. A., Simpson, Straznicky, P. V., and Krizan, D. V., "The Effect of Corrosion on the Durability and Damage Tolerance Characteristics of Longitudinal Fuselage Skin Splices," *Proceedings of 1998 USAF Aircraft Structural Integrity Program Conference*, 1998.

[17]Bellinger, N. C., Komorowski, J. P., and Gould, R. W., "Corrosion Pillowing Cracks in Fuselage Joints," *Proceedings of the Second Joint NASA/FAA/DoD Conference on Aging Aircraft*, NASA Langley Research Center, 1998.

[18]Manning, S. D., and Yang, J. N., "Advanced Durability Analysis, Volume I—Analytical Methods," Air Force Flight Dynamics Labs., Rept. AFWAL-TR-86-3017, Wright–Patterson AFB, OH, July 1987.

[19]MIL-HDBK-17-1E, *Polymer Matrix Composites*, Vol. 1, Dept. of Defense, 1997, pp. 8–22.

[20]Lawless, J. F., *Statistical Models and Methods for Lifetime Data*, Wiley, New York, 1982, p. 431.